Arabian Journal of Chemistry (2015) **xxx**, xxx–xxx

King Saud University

Arabian Journal of Chemistry

www.ksu.edu.sa
www.sciencedirect.com

ORIGINAL ARTICLE

Properties of electrodeposited functional Ni–Fe/AlN nanocomposite coatings

Manoj Kumar Tripathi, V.B. Singh *

Department of Chemistry, Centre of Advanced Study, Banaras Hindu University, Varanasi 221005, India

Received 2 October 2015; accepted 23 November 2015

KEYWORDS

Electrodeposition;
Ferromagnetic;
Nanocomposite;
Microstructure;
Aluminium nitride (AlN);
N,N-dimethylformamide

Abstract Ni–Fe/AlN nanocomposite coatings were electrodeposited from sulphamate based electrolyte in N,N-dimethylformamide solvent. The conditions of maximum particulate incorporation into the matrix were optimized. The coatings were characterized by Scanning electron microscopy (SEM), Energy dispersive analysis of X-ray (EDAX), X-ray diffractometry (XRD), and Vicker's microhardness tester. The reinforcement of matrix with nano-AlN rendered superior microhardness (up to 560 HV) to the nanocomposites over monolithic Ni and Ni–Fe alloy deposits. Incorporation of aluminium nitride (AlN) particles in the Ni–Fe alloy matrix under optimum condition was recorded up to 23.2 wt%. Magnetic measurements revealed soft ferromagnetic behaviour of the deposit with marked tendency towards superparamagnetism.

1. Introduction

It is increasingly recognized that new applications for materials require functions and properties that are not achievable with monolithic materials. Therefore, in recent years, much attention is being paid on the development of new and hybrid materials with the combination of dissimilar ones for these new applications (Moya et al., 2007; Catauro et al., 2014). The properties of these materials are not only sum of individual contributions of both the phases, but the role of the inner interfaces could be important (Sanchez et al., 2005). Metal matrix composites are considered as one of such materials to meet these requirements. The Metal Matrix Nanocomposites (MMNCs), compared to its traditional bulk counterpart, are more attractive due to their superior properties such as higher hardness (Singh and Singh, 2014), improved wear and corrosion resistance (Lekka et al., 2010), outstanding magnetic property (Sekino et al., 1996), good electrical and catalytic properties (Low et al., 2006). There are various methods such as physical vapour deposition (PVD), chemical vapour deposition (CVD), electrodeposition, lithography, sol–gel, and others to fabricate such composite materials out of which electrodeposition is considered to be one of the most versatile and important techniques, owing to precisely controlled near room temperature operation, rapid deposition rates and cost.

Literature survey reveals that a variety of particulates (SiC, Al_2O_3, TiO_2, TiC, etc.) has been added to the plating baths to form metal composite coatings (Wang and Wei, 2003; Singh and Singh, 2014). Our earlier studies (Chaudhari and Singh, 2015; Singh et al., 2012, 2013, 2015; Tripathi et al., 2013, 2015a) have demonstrated that the strength and corrosion resistance can be significantly enhanced by introducing second phase ceramic particles into the Ni and Ni–Fe matrix. It has been reported that decreasing particle size improves the mechanical properties of metal matrix composites (Yan et al., 2007) and nano-sized reinforcements enhance the mechanical

* Corresponding author.
E-mail address: vijaybs@bhu.ac.in (V.B. Singh).
Peer review under responsibility of King Saud University.

Production and hosting by Elsevier

http://dx.doi.org/10.1016/j.arabjc.2015.11.006
1878-5352

properties more effectively than those of the micron-sized ones (Zhou et al., 2014).

Among various ceramic particles, aluminium nitride (AlN) is an attractive candidate for the reinforcement because it possesses exceptional combination of functional properties, such as optical transparency, high thermal conductivity, substantially high hardness (24 GPa) and elastic modulus and piezoelectric activity. It is a covalent, non-metallic, refractory ceramic with high melting point and stable thermally as well as chemically (Pierson, 1996). In addition, it is good electrical insulator, hard and strong material. The quantity and distribution of such nanometric AlN dispersoids largely can dictate the mechanical properties of the composites. Owing to its high thermal conductivity, good insulating properties and high dielectric constant, AlN is an important wide band gap semiconductor and is ideally suitable for applications in microelectronics (Chen et al., 2010, 2012, 2013; Sinha et al., 2009). Therefore, it is important and interesting to develop nano-sized particle reinforced composites with superior mechanical properties.

Ni–Fe alloys play very important role in modern engineering. Ni rich Ni–Fe permalloys are particularly interesting because of their electrical and soft magnetic properties with a very high magnetic permeability (Ustinovshikov and Shabanova, 2013). Soft magnetic materials, in particular Ni–Fe alloys, are of prime importance in magnetic materials research due to their extraordinary magnetic, mechanical and electrical characteristics (Chicinas et al., 2005) better than those of pure Fe (Peng et al., 2008) and addition of AlN into the Ni–Fe alloy matrix can cause a significant change in characteristics of the resulting composite. Only limited studies have been reported on the surface morphology, microstructure, hardness, electrical, magnetic and electrochemical properties of electrodeposited nanostructured MMCs thin films embedding AlN nanoparticles. However, the investigations on addition of nano-sized AlN particles into conventional metal materials to fabricate the nano-sized AlN particle reinforced metal matrix composites are still rare, especially into the Ni–Fe alloy. Therefore, it is important and attractive to investigate the fabrication and strengthening mechanisms of the nano-sized AlN particles reinforced Ni–Fe matrix composites.

Organic solvent bath has been chosen purposefully for electrolysis since the failure of polycrystalline face-centred-cubic (FCC) Ni and its alloys due to hydrogen embrittlement are often sudden and unpredictable (Jothi et al., 2015). The hydrogen gets codeposited along with the metal during electrodeposition from aqueous media and causes microstructural changes (Nakahara and Felder, 1982) in the deposits and thus affects its properties and performance. Therefore, curiosity arises for the search of such a solvent which minimizes this undesired effect of the hydrogen. The possible solution is seen with use of either organic solvents or the ionic liquids. Ionic liquids pose difficulty in their synthesis, availability and cost and on the other hand organic solvents are easily available with a variety of functional groups and also are cost effective compared to the ionic liquids. Since aluminium based ceramics are difficult to codeposit with the metal matrix due to their instability (hydrolysis) in aqueous media, N,N-dimethylformamide (DMF), which has no active hydrogen is selected as medium in this investigation.

Present investigation deals with the microstructure, hardness, electrical, thermal, magnetic and electrochemical properties of the electrodeposited Ni–Fe alloy reinforced with the nano-sized AlN particles.

2. Experimental

2.1. Electrodeposition

Nickel sulphamate tetrahydrate (Fluka-Aldrich), ferrous sulphate heptahydrate (Fisher-Scientific India), boric acid (Qualigens Fine Chemicals India), AlN nanopowder (Sigma–Aldrich, particle size < 100 nm) and N,N-dimethylformamide (Fluka-Aldrich) were used in the bath. All chemicals were of analytical grade and used as procured.

The bath composition and electrolysis conditions are given in Table 1. The required amount of electrolytes (nickel sulphamate 24.0 g, ferrous sulphate 4.0 g and boric acid 5.0 g) was mixed together with 100 mL of N,N-dimethylformamide (DMF) in the form of slurry which was then transferred to the electrolysis cell and the volume was made up to 200 mL by adding DMF. After dissolution of the electrolytes, 5 g of the AlN nanoparticles was added to the electrolyte solution. Before electrolysis the solution was stirred continuously with the help of DC regulated mechanical stirrer for 24 h at 45 ± 0.5 °C to get uniform suspension.

The electrolysis cell has an assembly of two parallel pure nickel anodes (2 cm × 2 cm × 0.5 cm) on either side of a centrally placed commercial copper (Cu-99.28% & Ni-0.72%) plate (2 cm × 1 cm × 0.2 cm) cathode. Electrodeposition was carried out using a thermostated water bath (Haake K15 with Haake DC30 control, Netherlands) at 45 ± 0.5 °C employing DC current density in the range of 0.5–5.0 A dm^{-2} for 20–90 min. The details of the electrolysis cell assembly, substrate preparation and working procedures are described elsewhere (Tripathi et al., 2015a).

2.2. Characterization

The phase composition and crystallographic structure of the as-deposited films were characterized by X-ray diffraction (XRD, Bruker D8 ADVANCE ECO) using Cu Kα radiation of wavelength 1.5418 Å. X-ray data were collected at a scan rate of 2°/min. The average crystallite sizes of the coatings were calculated from the diffraction peak widths (Scherrer equation), according to the equation:

$$D = 0.94\lambda/\beta\cos\theta \quad (1)$$

while the microstrain was calculated using the equation:

$$\eta = \beta/4\tan\theta \quad (2)$$

where 0.94 is the shape factor, λ is the X-ray wavelength, β is the line broadening at half the maximum intensity (FWHM) in radians, θ is the Bragg angle, D is the mean crystallite size, and η is the microstrain in the coatings.

Morphology of the deposits was examined by Scanning Electron Microscope (SEM, Philips XL20) and Atomic Force Microscope (AFM, NT-MDT SOLVER Next AFM/STM) in semi-contact mode. The compositional analysis was done spectrophotometrically (Tripathi et al., 2013) and it was further

Table 1 Electrodeposition parameters.

Parameter	Value
$Ni(SO_3NH_2)_2{\cdot}4H_2O$	120 g L^{-1}
$FeSO_4{\cdot}7H_2O$	2 g L^{-1}
H_3BO_3	25 g L^{-1}
$HCON(CH_3)_2$	Solvent
AlN nanopowder	5–20 g L^{-1}
Temperature	45 ± 0.5 °C
Current density	1–5 A dm^{-2}
Agitation	700 ± 20 rpm

Please cite this article in press as: Tripathi, M.K., Singh, V.B. Properties of electrodeposited functional Ni–Fe/AlN nanocomposite coatings. Arabian Journal of Chemistry (2015), http://dx.doi.org/10.1016/j.arabjc.2015.11.006

substantiated by Energy Dispersive X-ray Analysis (EDAX, JEOL 840A). In EDAX analysis usually 5–10 spots on the sample surface are selected randomly and the values are averaged. The microstructure of the composite coatings was examined under Transmission Electron Microscope (TEM, TECNAI G^2 FEI) at an accelerating voltage of 200 kV.

The hardness of the nanocomposite coatings was evaluated using Vickers diamond indentation tester (Shimadzu HMV-2) applying 25 g f (0.0980665 N) load for 10 s. All the indentations were made by applying the load perpendicular to the smooth, free surface of the coatings. A minimum of five measurements was taken for a sample to obtain a statistical average value for microhardness.

The magnetic measurements on the nanocomposites were done using fine powder (scraped from the substrate) on a Vibrating Sample Magnetometer (VSM, Lakeshore 735). The *M–H* data were recorded at 300 K while *M–T* was recorded between temperatures 500 K and 78 K at 1000 Oe applied magnetic field.

Thermal study of the samples was performed on DSC822^e Mettler Toledo equipment in the temperature range of 30–900 °C at a heating rate of 3 °C min^{-1}. Electrical resistivity of the samples was measured by the four-probe method with a Keithley Nanovoltmeter 2182A and Keithley Source-meter 2400 at 27 °C.

Polarization studies for nickel–iron alloy and composite deposition were carried out at 45 °C using a potentiostat (POS73 Wenking) by step-wise increase of 20 mV potential under mechanical agitation. Cu plate was used as working electrode and Pt foil as counter electrode. The potentials are reported with respect to Saturated Calomel reference electrode (SCE).

3. Results and discussion

3.1. Effect of current density

Out of several deposition parameters such as temperature, electrolyte concentration, particle bath load, and agitation current density is the most important one. It has pronounced effect on the particle incorporation, microstructure, morphology, crystallographic structure, and mechanical, electrical and magnetic properties of the deposits. The effect of applied current density on AlN particle incorporation in the deposits was investigated and is represented in Fig. 1. The figure depicts that initially on increasing current density the wt% incorporation of AlN particle in the deposits increases gradually, reaches the maximum, 23 wt% at 3.0 A dm^{-2} and then decreases to the limiting value symptotically.

It is conceived from the results that the particle incorporation follows Guglielmi's model (Guglielmi, 1972). Accordingly the particles suspended in the electrolyte solution get surrounded by the cations. Initially, when current is applied, the cation laden particles present in the vicinity of the cathode get adsorbed on the surface and then simultaneous reduction of cations on the bare cathode and on the surface of the particles results in the strong embrace of the particles in the metal film being deposited. As the current density is further increased, the particle incorporation is also increased, reaching the maximum at 3.0 A dm^{-2}. A further increase in the current density enhanced reduction of the metal cations while the particle transport from bulk to the cathode becomes diffusion controlled. As a result, the flux of particles compared to the flux of metal ions decreases, consequently the particle content of the deposit decreases.

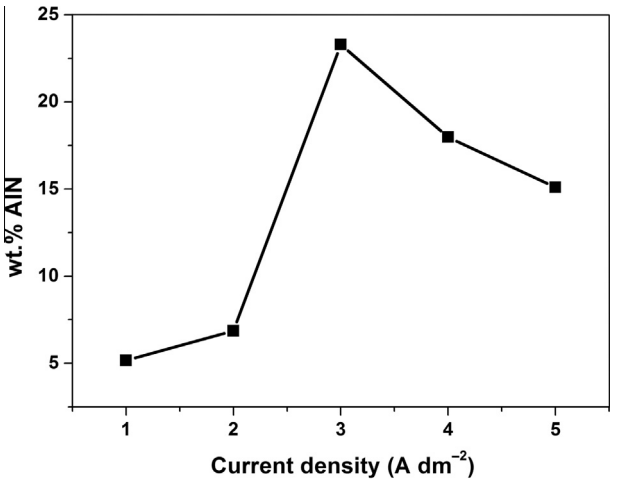

Figure 1 Effect of current density on wt.% incorporation of AlN particle in the deposits. (AlN particles 5 g/L.)

3.2. Phase structure (XRD analysis)

Fig. 2 shows the X-ray diffraction patterns of AlN nanopowder (Fig. 2a) and the Ni–Fe/AlN composite coatings (Fig 2b–f) prepared at various current densities. The XRD pattern of AlN powder reveals typical broad intense lines appearing at 2θ = 33.22 (100), 36.01 (002), 37.93 (101), 49.80 (102), 59.37 (2−10), 66.01 (103), 69.75 (200), 71.43 (2−12), 72.65 (201), 76.38 (004), 81.09 (202) and 85.87 (104) corresponding to the hexagonal structure with $a = b = 3.109$ Å and $c = 4.988$ Å [JCPDF 65-1902]. On the other hand the XRD patterns of the composite coatings show typical peaks of the substrate, Ni–Fe alloy and few feeble peaks of the AlN. The

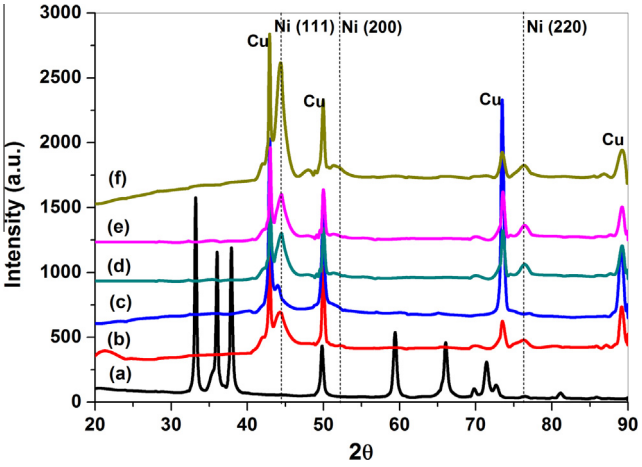

Figure 2 XRD patterns of AlN powder (a), Ni–Fe/AlN composite prepared at current density 1.0 A dm^{-2} (b), 2.0 A dm^{-2} (c), 3.0 A dm^{-2} (d), 4.0 A dm^{-2} (e) and 5.0 A dm^{-2} (f). (AlN particles 5 g/L.)

Table 2 Crystallite size and microstrain.

Current density (A dm^{-2})	Crystallite size (nm)	Microstrain
1.0	14.7 ± 1	0.0065
2.0	11.5 ± 1	0.0083
3.0	12.2 ± 1	0.0136
4.0	10.1 ± 1	0.0095
5.0	9.3 ± 1	0.0115

peaks of matrix can be indexed to (111), (200) and (220) crystal planes of FCC type Ni–Fe alloy.

The crystallite size of the as deposited samples was calculated from the Scherrer's equation with (111) peaks in the XRD patterns (Fig. 2b–f) after subtracting the instrumental broadening (Table 2) which was found around 9–15 nm. The maximum microstrain was found in the composite prepared at current density 3.0 A dm^{-2} while the minimum value was obtained for that at current density 1.0 A dm^{-2}. Observed maximum value of microstrain can be ascribed to the maximum incorporation of the AlN particles causing more deformation of the matrix grains. The results are consistent with our earlier report (Tripathi et al., 2015a,b).

3.3. Morphology

3.3.1. SEM

Fig. 3 represents typical fine granular and nearly smooth surface morphology of the Ni–Fe/AlN deposits obtained at current density 3.0 A dm^{-2}. The cluster of AlN particles can be seen easily on the surface. There are some holes on the surface which might have formed due to detachment of incompletely adhered AlN clusters.

The cross-sectional SEM image of the coating is shown in Fig. 4. The matrix grains are clearly visible in the deposits (Fig. 4a). There is good adherence of the coatings on the substrate surface. The coating thickness was estimated by cross-sectional SEM and was found between 20 μm and 40 μm. It can be seen from Fig. 4b that the larger grains are of uniform size with semi-spherical or oval shape. The size of these grains varies between 4 μm and 9 μm. Each larger grain also consists of many tiny grains with size less than 0.5 μm and these grains are closely packed.

3.3.2. AFM

Fig. 5 shows the AFM image of Ni–Fe/AlN composite coating obtained at current density 2.0 A dm^{-2} (Fig. 5a) and 3.0 A dm^{-2} (Fig. 5b) from a particle bath load of 5 g L^{-1}. A compact nodular morphology of the surface can be examined in the figure. The nodules are cluster of a large number of grains and the grains consist of the aggregation of many small crystallites, which is consistent with the results of XRD and SEM. The grain analysis of the surface (10 μm × 10 μm) showed that the clusters are of various sizes ranging between 150 nm and 1105 nm. The grain size obtained from the grain analysis of surface (1 μm × 1 μm) for fine grains, ranged between 9 nm and 34 nm. Roughness analyses of the surface revealed an average surface roughness (R_a) 25.525 nm and the root-mean square roughness (R_q) 33.758 nm.

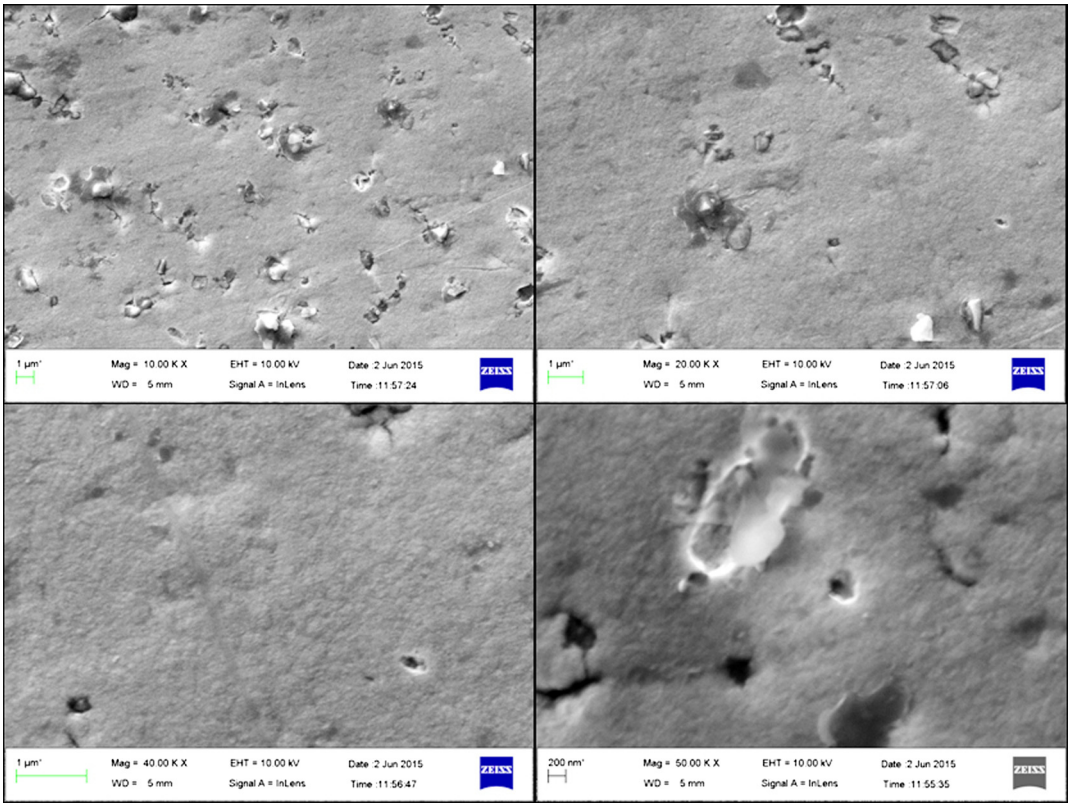

Figure 3 SEM morphology of Ni–Fe/AlN composite coating deposited at current density 3.0 A dm^{-2}. (AlN particles 5 g/L.)

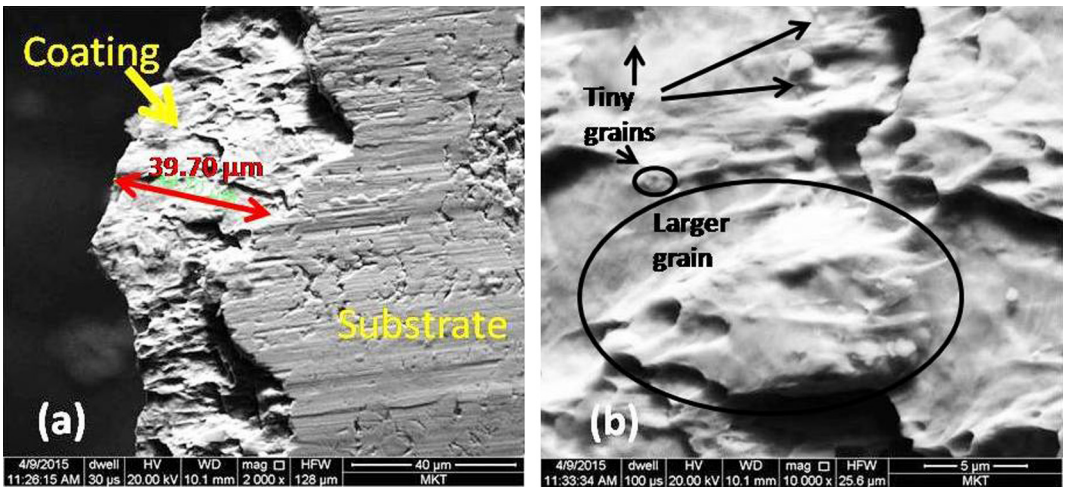

Figure 4 Cross-sectional SEM of Ni–Fe/AlN nanocomposite on the substrate (a) and the coating (b) prepared at 3.0 A dm^{-2} from a bath having 5 g L^{-1} AlN nanoparticles.

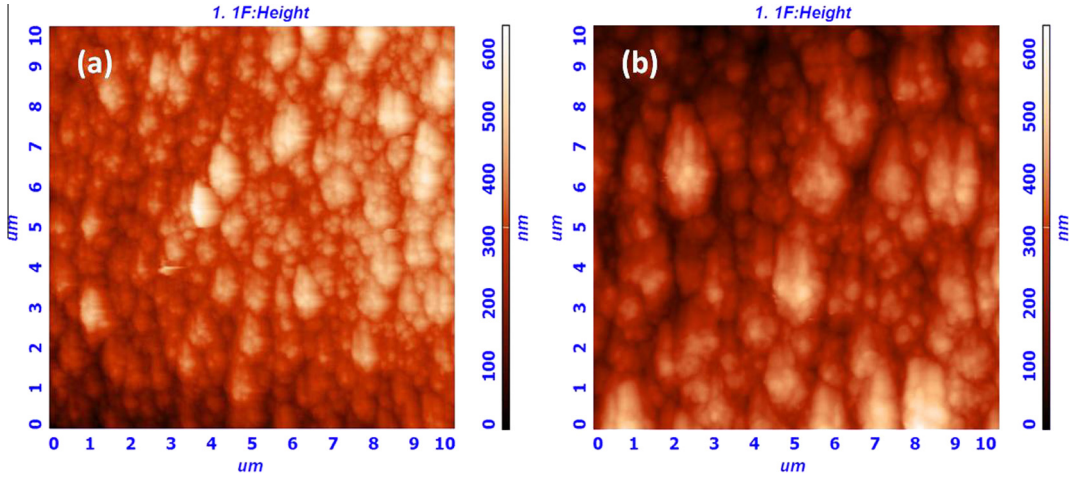

Figure 5 AFM image of Ni–Fe/TiN composite prepared at 2.0 A dm^{-2} (a) and 3.0 A dm^{-2} (b) from a bath with load of 5 g L^{-1} of AlN nanoparticles.

3.4. Microstructure (TEM)

A typical microstructure and corresponding SAED pattern of the as prepared Ni–Fe/AlN electrodeposit are shown in Fig. 6. The bright field image demonstrates fine granular structure of the deposits. The average grain size seems to be ~14 ± 2 nm which is consistent with the crystallite size calculated from the XRD data. The deposits are dense and compact without dislocations, twins and other defects except grain boundaries (GB).

The SAED pattern (inset of Fig. 6) of the deposit consists of continuous rings in a specific manner, which confirms polycrystalline FCC crystallographic structure of the coatings. The rings observed in the SAED pattern are assigned as to correspond to (111), (200), (220), (311) and (331) planes of Ni–Fe alloy.

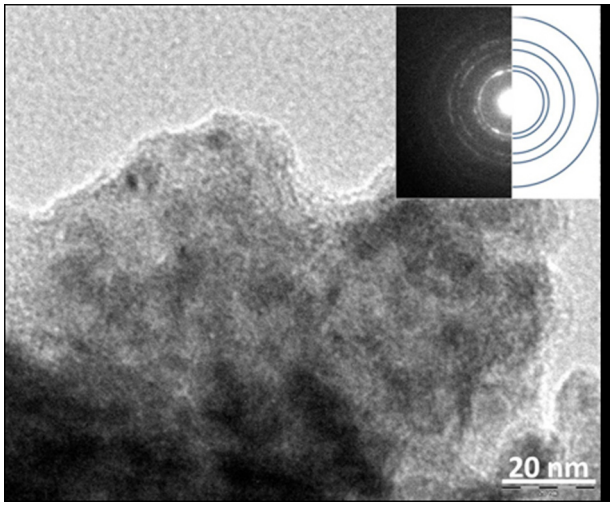

Figure 6 Microstructure (TEM) of Ni–Fe/AlN deposit along with SAD pattern. (3.0 A dm^{-2}; AlN particles 5 g/L.)

3.5. Microhardness

Microhardness of the composite deposits obtained at different deposition current density is shown in Fig. 7. It can be seen

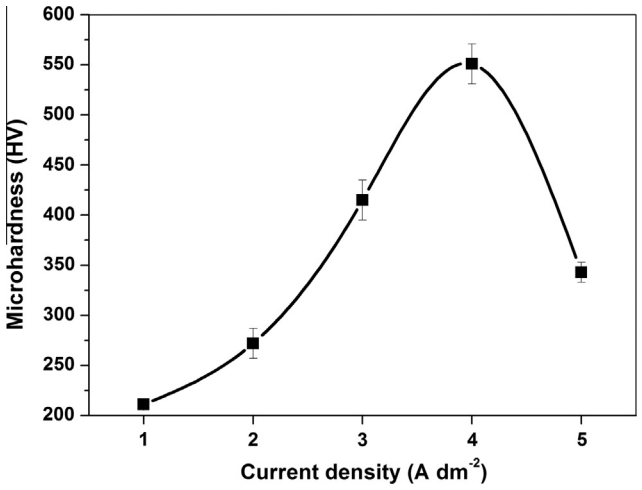

Figure 7 Variation of microhardness with current density. (AlN particles 5 g/L.)

that the microhardness increases with increasing current density up to 4.0 A dm^{-2} and decreases thereafter. Among all the deposition variables, current density has the most pronounced effect on the microhardness of the deposits. As can be corroborated from Table 2, the crystallite size of the deposits is not influenced by the applied current density, but as illustrated in Fig. 1, the particle content differs greatly. The initial increase in microhardness is due to the incorporation of AlN particles up to current density 3.0 A dm^{-2}. It is intuitive that the maximum hardness achieved at 4.0 A dm^{-2} is presumably attributed to the synergistic effects of the incorporated particles and to the contribution of grain boundaries due to size confinement effect of current density.

Present results can be visualized in light of several reported strengthening mechanisms in MMC based on Al, such as Orowan strengthening, grain boundary strengthening and hardening due to the difference in thermal expansion coefficients between phase constituents (Ferguson et al., 2014; Schultz et al., 2011).

When the grain size becomes less than a certain value in the nano range (less than 50 nm), the grains become free from dislocation, and therefore, the dislocation mediated plastic deformation becomes hindered (Meyers et al., 2006; Kumar et al., 2003). At this nano-size level the contribution of grain boundaries to the microhardness dominates. Grain boundary mediated plastic deformation processes take place through grain boundary sliding, coble creep and grain rotation (Conrad, 2003). Keeping the above facts in view it can be considered that the incorporated AlN particles prevent grain boundary sliding and thus results into increase in the microhardness.

From the crystallite size calculations it is intuitive to arrive that the crystallite size of the matrix is much smaller than the AlN particles; therefore, in the composite coatings, all the AlN nanoparticles cannot be considered embedded entirely inside the matrix grains; instead they could be surrounded by several grains; consequently some of the matrix grain boundaries are replaced with particle–matrix interfaces. At these interfaces the AlN nanoparticles can strengthen the grain boundaries and hinder the plastic deformation (Bakhit and Akbari, 2012).

3.6. Magnetic property

The field-dependent magnetization (M–H hysteresis) curve of the Ni–Fe/AlN deposit (prepared at 2.0 A dm^{-2} from a bath load of 5 g L^{-1} of the AlN particles) at room temperature is represented in Fig. 8. Typical hysteresis is clearly observed which indicates ferromagnetic behaviour of the deposited composite. The composite has low coercivity (H_c = 28 G), very low magnetic remanence (M_r = 2.22 emu/g) and high saturation magnetization (M_s = 62.02 emu/g). Earlier we have reported the room temperature values H_c, M_r and M_s for the Ni–Fe alloy deposit (Tripathi et al., 2015b) as 61.2 G, 3.07 emu/g and 51.2 emu/g, respectively. In the present study, the values of H_c and M_r for Ni–Fe/AlN deposits are found comparatively very low. The difference in the values can be thought of due to the microstructure of the composite deposit (single domain grain size resulting in strong particle–particle interaction) and the nature of AlN particles. The presence of the hysteresis loop and small coercivity indicates the soft magnetic nature of the deposit but from the shape of the loop a marked signature of superparamagnetism can be recognized. The M_r/M_s value for the deposit is 0.035 which also supports the above inference (Couderchon and Tiers, 1982). The saturation of magnetic moment at very high fields (above 2 kG) reflects the random magnetic anisotropy (Chudnovsky and Serota, 1982) existing in the materials with crystallite size below 20 nm (Moustaïde et al., 1999). These results agree with our earlier observations (Tripathi et al., 2015b).

In order to substantiate the results of M–H hysteresis M–T measurements were also performed. The variation of magnetization with temperature at 0.1 T applied field is illustrated in Fig. 9 wherein the Curie temperature (T_C) was identified and was found to be ~540 K while in the case of Ni–Fe/TiN the value of T_C was found to be 590 K (Tripathi et al., 2015b). The bifurcation of FC and ZFC curves occurs at a temperature 297 K and they never meet below this temperature. The ZFC curve at lower temperatures goes down and above this temperature the curves coincide. Bifurcation between ZFC and FC curves is generally a characteristic feature of superparamagnetism, resulting from competing ferro- and antiferromagnetic pair interactions between the components. More specifically,

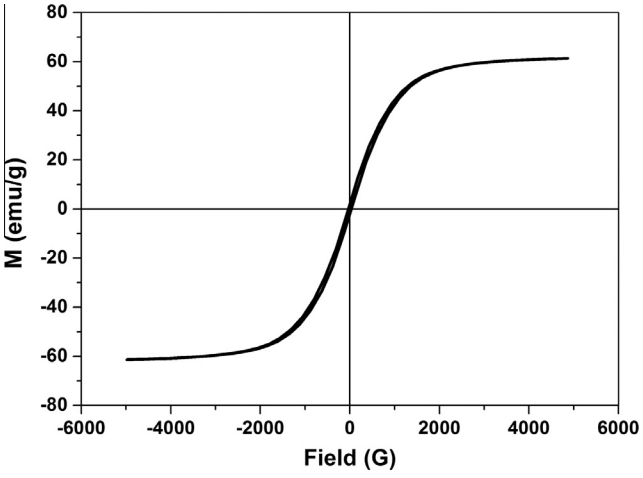

Figure 8 M–H curve for NFAN-2 measured at 300 K. (AlN particles 5 g/L.)

Please cite this article in press as: Tripathi, M.K., Singh, V.B. Properties of electrodeposited functional Ni–Fe/AlN nanocomposite coatings. Arabian Journal of Chemistry (2015), http://dx.doi.org/10.1016/j.arabjc.2015.11.006

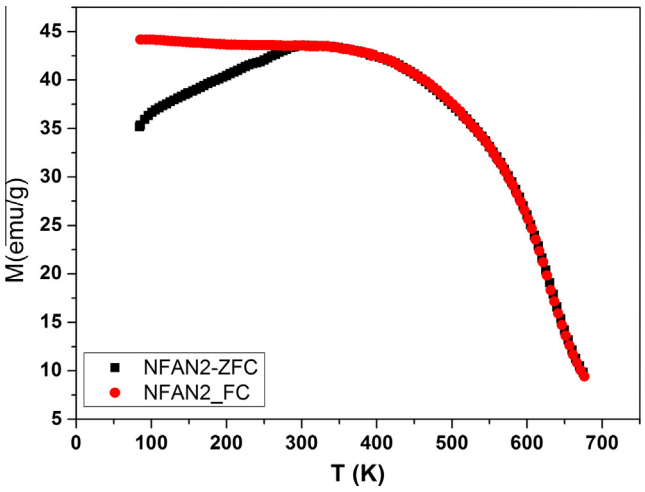

Figure 9 *M–T* (FC & ZFC) curve of NFAN-2. (AlN particles 5 g/L.)

below the bifurcation temperature irreversibility sets in and below the ZFC-peak temperature, the system passes to a mixed magnetic phase. It has been reported that the FC and ZFC curves start bifurcating at higher temperatures with the decrease in inter-particle separation (Sato et al., 2000; Morup et al., 1995). Above type of bifurcation is an impression of magnetic metastability as a consequence of blocked magnetic moments in superparamagnetic particles below T_B (blocking temperature). From these results it is apparent that the magnetic behaviour is superparamagnetism at the temperature above 270 K. There is a gradual increase in FC magnetization with decreasing temperature. The FC/ZFC measurements show typical superparamagnetic behaviour and the ZFC curve yields a cusp at 270 K, characteristic blocking temperature.

Present results of magnetic measurements can be discussed for magnetic materials, in terms of domain walls which play an important role. Upon application of a magnetic field, initially domain walls will tend to move reversibly, so that the domains that are magnetized with a component in the direction of the field grow at the expense of domains magnetized in opposite directions. Continuing to apply an increasing field the domain walls begin to move from their original positions irreversibly into new positions. Usually in this state the increase in magnetization with field is steeper and reaches the maximum and finally in the saturated magnetic state. Thus, coercivity in such materials generally increases with decreasing particle size or, in fully dense materials, with decreasing grain size. The nonmagnetic second phase particles and the grain boundaries are ought to have pinning effect on domain wall motion in nanocrystalline materials resulting in an increase in the coercivity. Soft magnetic materials usually possess high permeability and low coercive force and in general, their magnetic behaviour is governed by domain wall pinning at heterogeneities such as grain boundaries, surfaces, precipitates and inclusions.

3.7. Electrical resistivity

Electrical resistivity is an important physical property of the coatings which is responsible for many applications. However, the studies on the resistivity measurements of electrodeposited nanocomposite coatings are rarely reported. Therefore, the measurement was done for the Ni–Fe and Ni–Fe/AlN composite coatings. Fig. 10 depicts the measured apparent electrical resistivity of the composite coatings deposited at different current densities. The apparent electrical resistivity of the deposits was found to be of the order $10^{-8}\ \Omega$ cm. It can be seen, in the figure, that the electrical resistivity value of the coatings does not show a regular trend of variation with current density; in general, more or less it decreases with an increase in the deposition current density except at 5.0 A dm^{-2}. A correlation of electrical resistivity (Fig. 10) of the composite deposits with the particulate content (Fig. 1) and the crystallite size (Table 2) indicates that the particulate content in the deposits does not seem to affect the resistivity of the coatings, as very little variation in crystallite size of the coatings i.e. only few nm is observed; however, it is known that below a critical size limit (below 20 nm) any alteration in crystallite size poses drastic change in the properties of the nanomaterials (Cao, 2004). Therefore, explanation for the observed trend in the electrical resistivity of the composite can be alternatively looked into their crystallite size. The higher value of resistivity at initial deposition current density can be due to the larger crystallite size of the deposit where the grain boundaries offer increased resistance. As the deposition current density increases, the crystallite size decreases. Once the crystallite size becomes much below the critical limit, though the density of grain boundaries increases yet the crystallites/grains offer hopping conductance resulting in declined resistivity. The highest value of electrical resistivity offered by the deposits at the highest deposition current density seems due to the grain boundary segregation resulting from the diffusion controlled metal deposition. It is worth noting that the resistivity of the Cu-substrate and the Ni–Fe alloy (3.0 A dm^{-2}) was measured to be $2.5 \times 10^{-7}\ \Omega$ cm and $4.97 \times 10^{-8}\ \Omega$ cm, respectively. Thus a comparison of the apparent electrical resistivity between bulk Cu, Ni–Fe alloy and the Ni–Fe/AlN nanocomposites depicts that the nanocomposites offer much less resistivity than the bulk Cu and Ni–Fe alloy (Chaudhari and Singh, 2015; Tripathi et al., 2015a,c). Furthermore, there is almost marginal decrease in the electrical resistivity of the Ni–Fe matrix on

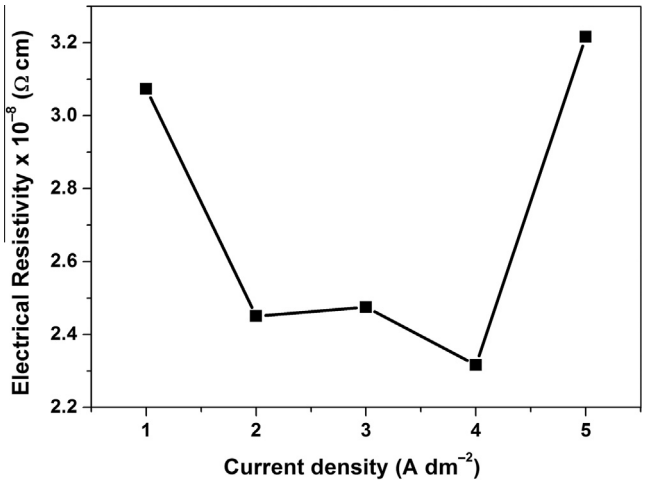

Figure 10 Apparent electrical resistivity of composites deposited at different current densities. (AlN particles 5 g/L.)

inclusion of the nano-AlN particles. Thus it can be conceived that there is negligible effect of AlN particle incorporation in the Ni–Fe alloy matrix.

Since resistivity has been measured at room temperature, therefore, the surface scattering may be ignored which is a temperature dependent phenomenon. In the present investigation the coatings have been prepared under such conditions that the presence of residual stress and dislocation is expected to be greatly reduced. Again, since the bath and the particles were fairly stable, the occlusion of any decomposition product in the composite or at the interfaces can be safely ignored. Such interfaces are known to decrease electrical resistivity (Singh and Singh, 2014).

The effect of size of nanostructures on electrical resistivity (conductivity) is complex (Cao, 2004) and based on surface scattering, quantized conduction, ballistic conduction, coulomb charging, tunnelling, size of band gap and change in microstructure. Moreover, in near absence of the literature pertaining to the resistivity of MMNCs, it is difficult to extend a definite mechanism to explain the observed results.

3.8. Electrochemical study

3.8.1. Polarization

In order to determine deposition potential of Ni–Fe alloy and the Ni–Fe/AlN nanocomposite, cathodic polarization studies were performed. Fig. 11 shows cathodic polarization curves for Ni–Fe alloy and Ni–Fe/AlN composite deposition. The curves show that the deposition potential of Ni–Fe alloy is ~600 mV cathodic (vs. SCE) while in the presence of AlN particles it shifts towards less cathodic direction by ~50 mV. From the polarization studies it is arrived that on addition of AlN nanoparticles to the Ni–Fe plating solution the current density of the Ni–Fe alloy deposition increases. A similar depolarization was observed in the presence of ceramic particles by several workers (Ibrahim et al., 2013; Tripathi et al., 2015a; Benea, 2009). However, such behaviour is not the same with other composite electrodeposition systems where addition of ceramic particles to the plating bath led to higher polarization of the deposition process (Vaezi et al., 2008; Shi et al., 2006). Therefore, from the present observed results it is enunciated that the AlN nanoparticles have facilitating/promoting effect on the Ni–Fe alloy deposition. It is speculated that when the particles are added to the plating bath, the metal cations are adsorbed on their surfaces and thus they increase the ionic transport towards cathode; consequently, the deposition potential shifts towards positive potentials and the associated current density increases due to the increased rate of metal deposition (Tuaweri and Wilcox, 2006). Secondly, the insulating AlN particles cover the cathode surface and thus the active cathode surface area decreases which can increase the associated current density.

3.8.2. Corrosion

To compare the corrosion resistance of the Ni–Fe alloy and Ni–Fe/AlN nanocomposite cathodic and anodic polarization studies were performed. The polarization curves for Ni–Fe alloy and Ni–Fe/AlN composite coatings (both prepared at 3.0 A dm^{-2}) in 3.5% NaCl solution are given in Fig. 12. The alloy and the composite both exhibited similar polarization curves with active and poor passive characteristic. The corrosion potential (E_{corr}) and corrosion current (I_{corr}) were determined extrapolating cathodic and anodic curves. The E_{corr} for Ni–Fe alloy was found to be −600 mV (SCE) and that for the Ni–Fe/AlN coating was −720 mV (SCE). Both the alloy and the composite show the tendency of passivation which might be due to the formation of a salt film on the surface. The I_{corr} for Ni–Fe coating was measured to be ~0.029 mA/cm^2 while that for the Ni–Fe/AlN nanocomposite coating was ~0.015 mA/cm^2. These current values indicate a marked decrease in corrosion of Ni–Fe/AlN nanocomposite coating compared to the Ni–Fe alloy coating. The improvement in corrosion resistance on incorporation of ceramic particles has been reported earlier by several workers (Zhu et al., 2011; Vaezi et al., 2008; Aruna et al., 2006; Li et al., 2005; Shi et al., 2006) which is in accordance with our results. On the other hand a reduction in corrosion resistance has also been reported in the presence of ceramic particles in the plating solution (Tripathi et al., 2015b; Lekka et al., 2009). It emerges out from the above discussions that the observed improved

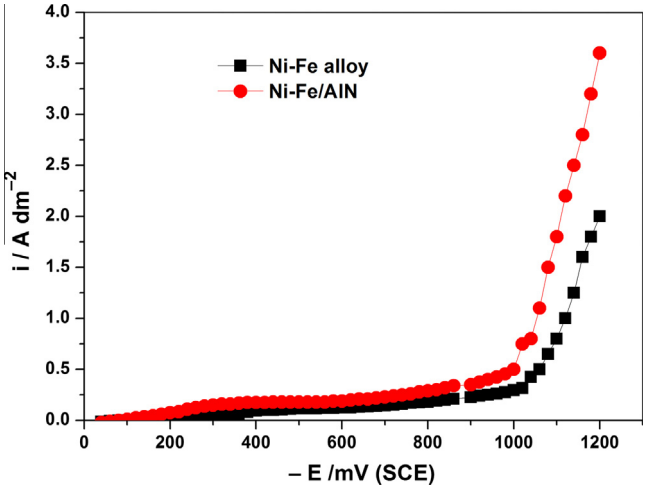

Figure 11 Cathodic polarization curves for Ni–Fe alloy and Ni–Fe/AlN composite deposition. (AlN particles 5 g/L.)

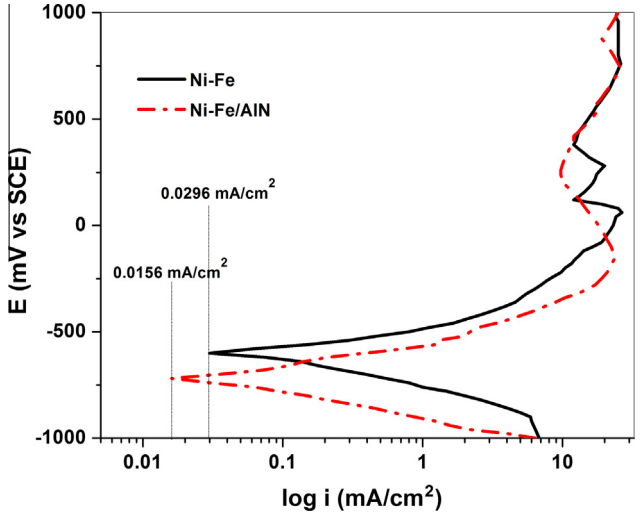

Figure 12 Corrosion behaviour of Ni–Fe alloy and Ni–Fe/AlN composite coatings. (3.0 A dm^{-2}; AlN particles 5 g/L.)

Please cite this article in press as: Tripathi, M.K., Singh, V.B. Properties of electrodeposited functional Ni–Fe/AlN nanocomposite coatings. Arabian Journal of Chemistry (2015), http://dx.doi.org/10.1016/j.arabjc.2015.11.006

corrosion resistance of the Ni–Fe/AlN nanocomposite coating over Ni–Fe alloy, in the present investigation, can be due to the positive effect of the incorporated AlN nanoparticles which being insulating in nature act as inert physical barrier to the initiation and development of defects. Additionally, the particles reduce the corrosion active surface area resulting in increased corrosion resistance of the nanocomposite coating. Moreover, the electrical resistivity of the Ni–Fe/AlN nanocomposite has been found to be lower than that of the Ni–Fe alloy which implies a more tendency towards corrosion. However, the results are unlike, which can be most likely caused by change in local microstructure around the occluded particles and their inertness. A comparison of Ni–Fe/AlN and Ni–Fe/TiN (Tripathi et al., 2015b) nanocomposite deposits shows that Ni–Fe/AlN nanocomposites are more resistant to corrosion than both the Ni–Fe alloy and Ni–Fe/TiN composite coatings.

4. Conclusions

The Ni–Fe/AlN nanocomposite was successfully electrodeposited and systematically investigated in this work. The XRD, TEM and AFM results indicated formation of nanostructured composite deposits. The crystallite size of the deposits ranged between 8 nm and 14 nm and the lattice strain was calculated to be < 0.014. At optimum conditions a maximum of 23.2 wt.% AlN nano-particulate was incorporated in the coatings. Ferromagnetic behaviour of the deposits with a marked tendency towards superparamagnetism was observed. FCC structure was observed for both the alloy and the composites with (1 1 1) preferred orientation. The Ni–Fe matrix reinforced with AlN nanoparticles exhibited superior microhardness (up to 560 HV), increased conductivity and increased corrosion resistance than the parent alloy.

Acknowledgements

The Council of Scientific and Industrial Research (CSIR) (01 (2678)-EMR-II), New Delhi, India) and the University Grants Commission (UGC, New Delhi, India) are greatly acknowledged for financial support and providing fellowship. Prof. R.K. Mandal (IIT-BHU) and Prof. O.N. Srivastav (Deptt. of Physics, BHU) are thanked for providing microhardness testing and TEM Facility.

References

Aruna, S.T., Bindu, C.N., Selvi, V.E., Grips, W.V.K., Rajam, K.S., 2006. Synthesis and properties of electrodeposited Ni/ceria nanocomposite coatings. Surf. Coat. Technol. 200, 6871–6880.

Bakhit, B., Akbari, A., 2012. Effect of particle size and codeposition technique on hardness and corrosion properties of Ni–Co/SiC composite coatings. Surf. Coat. Technol. 206, 4964–4975.

Benea, L., 2009. Electrodeposition and tribocorrosion behaviour of ZrO_2–Ni composite coatings. J. Appl. Electrochem. 39, 1671–1681.

Cao, G., 2004. Nanostructures and Nanomaterials: Synthesis, Properties and Applications. Imperial College Press, London WC2H 9HE, p. 371.

Catauro, M., Bollino, F., Papale, F., Giovanardi, R., Veronesi, P., 2014. Corrosion behaviour and mechanical properties of bioactive sol–gel coatings on titanium implants. Mater. Sci. Eng. C 43, 375–382.

Chaudhari, A.K., Singh, V.B., 2015. Studies on electrodeposition, microstructure and physical properties of Ni–Fe/In_2O_3 nanocomposite. J. Electrochem. Soc. 162, D341–D349.

Chen, C., Gao, S., Tang, G.S., Fu, H.D., Wang, G.Y., Song, C., Zeng, F., Pan, F., 2013. Effect of electrode materials on AlN-based bipolar and complementary resistive switching. ACS Appl. Mater. Interf. 5, 1793.

Chen, C., Gao, S., Tang, G.S., Song, C., Zeng, F., Pan, F., 2012. Cu-embedded AlN-based nonpolar nonvolatile resistive switching memory. IEEE Electron. Dev. Lett. 33, 1711.

Chen, C., Yang, Y.C., Zeng, F., Pan, F., 2010. Bipolar resistive switching in Cu/AlN/Pt nonvolatile memory device. Appl. Phys. Lett. 97, 083502.

Chicinas, I., Geoffroy, O., Isnard, O., Pop, V., 2005. Soft magnetic composite based on mechanically alloyed nanocrystalline Ni_3Fe phase. J. Magn. Magn. Mater. 290–291 (2005), 1531–1534.

Chudnovsky, E.M., Serota, R.A., 1982. Spin-glass and ferromagnetic states in amorphous solids. Phys. Rev. B 26, 2697(R)–2699(R).

Conrad, H., 2003. Grain size dependence of the plastic deformation kinetics in Cu. Mater. Sci. Eng. A 341, 216–228.

Couderchon, G., Tiers, J.F., 1982. Some aspects of magnetic properties of Ni–Fe and Co–Fe alloys. J. Magn. Magn. Mater. 26, 196–214.

Ferguson, J.B., Lopez, H.F., Rohatgi, P.K., Cho, K., Kim, C.S., 2014. Impact of volume fraction and size of reinforcement particles on the grain size in metal-matrix micro and nanocomposites. Metall. Mater. Trans. A 45, 4055–4061.

Guglielmi, N., 1972. Kinetics of the deposition of inert particles from electrolyte baths. J. Electrochem. Soc. 119, 1009–1012.

Ibrahim, M.A.M., Kooli, F., Alamri, S.N., 2013. Electrodeposition and characterization of Ni–TiN microcomposite coatings. Int. J. Electrochem. Sci. 8, 12308–12320.

Jothi, S., Croft, T.N., Brown, S.G.R., 2015. Multiscale multiphysics model for hydrogen embrittlement in polycrystalline nickel. J. Alloys Compd. 645, S500–S504.

Kumar, K.S., Swygenhoven, H.V., Suresh, S., 2003. Mechanical behaviour of nanocrystalline metals and alloys. Acta Mater. 51 (2003), 5743–5774.

Lekka, M., Zanella, C., Klorikowska, A., Bonora, P.L., 2010. Scaling-up of the electrodeposition process of nano-composite coating for corrosion and wear protection. Electrochim. Acta 55, 7876–7883. http://dx.doi.org/10.1016/j.electacta.2010.02.081.

Lekka, M., Koumoulis, D., Kouloumbi, N., Bonora, P.L., 2009. Mechanical and anticorrosive properties of copper matrix micro- and nano-composite coatings. Electrochim. Acta 54, 2540–2546.

Li, J., Sun, Y., Sun, X., Qiao, J., 2005. Mechanical and corrosion-resistance performance of electrodeposited titania–nickel nanocomposite coatings. Surf. Coat. Technol. 192, 331–335.

Low, C.T.J., Wills, R.G.A., Walsh, F.C., 2006. Electrodeposition of composite coatings containing nanoparticles in a metal deposit. Surf. Coat. Technol. 201 (2006), 371–383.

Meyers, M.A., Mishra, A., Benson, D.J., 2006. Mechanical properties of nanocrystalline materials. Prog. Mater. Sci. 51, 427–556.

Morup, S., Bodker, F., Hendriksen, P.V., Linderoth, S., 1995. Spin-glass-like ordering of the magnetic moments of interacting nano-sized maghemite particles. Phys. Rev. B Cond. Mater. 52, 287–294.

Moustaïde, A., Berraho, R., Sayouri, S., Hassini, A., 1999. Magnetic and random anisotropy studies in amorphous $Fe_{76-x}Ni_xCr_4B_{12}Si_8$ ($0 \leqslant x \leqslant 10$). Phys. B 270, 11–16.

Moya, J.S., Esteban, S.L., Pecharromán, C., 2007. The challenges of ceramic/metal microcomposites and nanocomposites. Prog. Mater. Sci. 52, 1017–1090. http://dx.doi.org/10.1016/j.pmatsci.2006.09.003.

Nakahara, S., Felder, E.C., 1982. Defect structure in nickel electrodeposits. J. Electrochem. Soc. 129, 45–49.

Peng, D.L., Sumiyama, K., Kumagai, K., Yamabuchi, T., Kobayashi, D., Hihara, T., 2008. Magnetic and electrical characteristics in dense Fe–Ni alloy cluster-assembled films prepared by energetic cluster deposition. J. Mater. Res. 23, 189–197. http://dx.doi.org/10.1557/JMR.2008.0018.

Pierson, H.O., 1996. Handbook of Refractory Carbides and Nitrides: Properties, Characteristics, Processing and Applications. Noyes Publications, Westwood, New Jersey, USA.

Sanchez, C., Julian, B., Belleville, P., Popall, M., 2005. Applications of hybrid organic–inorganic nanocomposites. J. Mater. Chem. 15, 3559–3592.

Sato, M., Kohiki, S., Hayakawa, Y., Sonda, Y., Babasaki, T., Deguchi, H., Mitome, M., 2000. Dilution effect on magnetic properties of Co_3O_4 nanocrystals. J. Appl. Phys. 88, 2771. http://dx.doi.org/10.1063/1.1287769.

Schultz, B., Ferguson, J.B., Rohatgi, P., 2011. Microstructure and hardness of Al_2O_3 reinforced Al–Mg composites fabricated by reactive wetting and stir mixing. Mater. Sci. Eng. A 530, 87–97.

Sekino, T., Nakajima, T., Niihara, K., 1996. Mechanical and magnetic properties of nickel dispersed alumina-based nanocomposite. Mater. Lett. 29, 165–169.

Shi, L., Sun, C., Gao, P., Zhou, F., Liu, W., 2006. Mechanical properties and wear and corrosion resistance of electrodeposited Ni–Co/SiC nanocomposite coating. Appl. Surf. Sci. 252, 3591–3599.

Singh, D.K., Tripathi, M.K., Singh, V.B., 2012. Preparation of Ni–TiC nanocomposites by electrolytic codeposition from a nonaqueous bath and their characterization. J. Electrochem. Soc. 159, D469–D472.

Singh, D.K., Tripathi, M.K., Singh, V.B., 2013. Electrodeposition and characterization of Ni–WC composite coating from non-aqueous bath. Int. J. Mater. Sci. Appl. 2, 68–73.

Singh, D.K., Tripathi, M.K., Singh, V.B., 2015. Electrolytic preparation of Ni-B_4C composite coating and its characterization. J. Mater. Eng. Perform. 24, 1213–1219.

Singh, V.B., Singh, D.K., 2014. An overview on the preparation, characterization and properties of electrodeposited metal matrix nanocomposites. Nanosci. Technol. 1, 1–20, < http://symbiosisonlinepublishing.com/nanoscience-technology/nanoscience-technology20.php > .

Sinha, N., Wabiszewski, G.E., Mahameed, R., Felmetsger, V.V., Tanner, S.M., Carpick, R.W., Piazza, G., 2009. Piezoelectric aluminum nitride nanoelectromechanical actuators. Appl. Phys. Lett. 95, 053106.

Tripathi, M.K., Singh, D.K., Singh, V.B., 2013. Electrodeposition of Ni–Fe/BN nanocomposite coatings from a non-aqueous bath and their characterization. Int. J. Electrochem. Sci. 8, 3454–3471.

Tripathi, M.K., Singh, D.K., Singh, V.B., 2015a. Microstructure and properties of electrochemically deposited Ni–Fe/Si_3N_4 nanocomposites from a DMF bath. J. Electrochem. Soc. 162, D87–D95.

Tripathi, M.K., Singh, V.B., Singh, H.K., 2015b. Structure and properties of electrodeposited functional Ni–Fe/TiN nanocomposite coatings. Surf. Coat. Technol. 278, 146–156.

Tripathi, M.K., Singh, D.K., Singh, V.B., 2015c. Response to ''Comment on 'Microstructure and Properties of Electrochemically Deposited Ni–Fe/Si_3N_4 Nanocomposites from a DMF Bath'[J. Electrochem. Soc., 162, D87 (2015)]''. J. Electrochem. Soc. 162 (8), Y7. http://dx.doi.org/10.1149/2.0391508jes.

Tuaweri, T.J., Wilcox, G.D., 2006. Behaviour of Zn–SiO_2 electrodeposition in the presence of N,N-dimethyldodecylamine. Surf. Coat. Technol. 200, 5921–5930.

Ustinovshikov, Y., Shabanova, I., 2013. A study of microstructures responsible for the emergence of the invar and permalloy effects in Fe–Ni alloys. J. Alloys Compd. 578, 292–296. http://dx.doi.org/10.1016/j.jallcom.2013.06.039.

Vaezi, M.R., Sadrnezhaad, S.K., Nikzad, L., 2008. Electrodeposition of Ni–SiC nanocomposite coatings and evaluation of wear and corrosion resistance and electroplating characteristics. Colloids Surf. A: Physicochem. Eng. Asp. 315 (2008), 176–182.

Wang, S., Wei, W.J., 2003. Kinetics of electroplating process of nanosized ceramic particle/Ni nanocomposite. Mater. Chem. Phys. 78 (2003), 574–580.

Yan, Y.W., Geng, L., Li, A.B., 2007. Experimental and numerical studies of the effect of particle size on the deformation behaviour of the metal matrix composites. Mater. Sci. Eng. A 448, 315–325.

Zhou, D., Qiu, F., Wang, H., Jiang, Q., 2014. Manufacture of nanosized particle-reinforced metal matrix composites: a review. Acta Metall. Sin. (Eng. Lett.) 27, 798–805. http://dx.doi.org/10.1007/s40195-014-0154-z.

Zhu, X.B., Cai, C., Zheng, G.Q., Zhang, Z., Li, J.F., 2011. Electrodeposition and corrosion behaviour of nanostructured Ni–TiN composite films. Trans. Nonferr. Met. Soc. China 21, 2216–2224.

Please cite this article in press as: Tripathi, M.K., Singh, V.B. Properties of electrodeposited functional Ni–Fe/AlN nanocomposite coatings. Arabian Journal of Chemistry (2015), http://dx.doi.org/10.1016/j.arabjc.2015.11.006